Journal of the Optical Society of Korea, Vol. 7, No. 3, September 2003, pp. 188-192

Modal Characteristics of Photonic Crystal Fibers

Yong-Jae Lee*, Dae-Sung Song, Se-Heon Kim, Jun Huh, and Yong-Hee Lee

Department of Physics, Korea Advanced Institute of Science and Technology, Daejeon 305-701, KOREA

(Received March 6, 2003)

The modal characteristics of the photonic crystal fibers are analyzed using the reliable and efficient plane wave expansion method. The mode profile, effective index and group velocity dispersion are obtained by solving Maxwell's vector wave equations without any approximation. The zero dispersion condition of a photonic crystal fiber is derived over a wide range of wavelengths. Higher-order modes are also easily found as a by-product of the plane wave expansion method. This method can be used to quickly and accurately design various optical properties of photonic crystal fibers.

OCIS codes : 060.0060, 060.2280.

I. INTRODUCTION

Recently, various photonic crystal based devices have been constructed [1,2]. Among these devices, photonic crystal fibers (PCFs) have many interesting characteristics. Unlike conventional step index fibers, PCFs can support a single mode over a wide range of wavelengths [3] and they have a large effective core area retaining the single mode [4]. PCFs based on air hole arrays have received particular attention on account of their manufacturability. Recently, the guiding property of PCFs has been successfully applied to single-transverse-mode vertical cavity surface emitting lasers [5].

Various theoretical methods have been employed to understand the characteristics of PCFs. In an early theoretical study, Ferrando et al. modeled PCFs using the full vector technique widely used for conventional fibers [6]. This model was subsequently simplified into scalar and vector models that achieved excellent calculation efficiency by using Hermite-Gaussian functions [7,8]. Although this simplified method gives greatly improved calculation speed, it cannot correctly handle structures with abrupt index variations in consequence of the approximation on the Maxwell equations. The finite element method (FEM) has also been used to model PCFs [9], but FEM calculations require huge computation power to obtain accurate results. The finite-difference time-domain (FDTD) method is another technique that can accurately model PCFs, but FDTD calculations require prohibitively long computation times. Therefore, a fast and accurate method for modeling PCFs would be of great benefit.

II. EFFICIENT METHODOLOGY AND RESULTS

To save the computation power without sacrificing accuracy, we use the plane wave expansion method with the electromagnetic energy functional to model PCFs. This method has been widely used to analyze the band structures and modal characteristics of photonic crystals [10–12]. The wave equation employed here is basically the vector eigenvalue equation of a Maxwell Hermitian operator :

$$\nabla \times \left(\frac{1}{\varepsilon(\vec{r})} \nabla \times \vec{H}(\vec{r}) \right) = \left(\frac{\omega}{c} \right)^2 \vec{H}(\vec{r}) \qquad (1)$$

where $\varepsilon(\vec{r})$ is the position-dependent dielectric constant, ω is an eigen frequency, and c is the speed of light. We assume the permeability μ to be unity. Note that no approximation is assumed in this full vector wave equation. For a given Bloch wavevector $\vec{\beta}$, the magnetic field $\vec{H}(\vec{r})$ is decomposed into plane waves having some reciprocal-lattice vectors $\vec{G}_m$,

$$\vec{H}(\vec{r}) = e^{i(\vec{\beta}\cdot\vec{r}-\omega t)} \sum_{m=1}^{N} h_m e^{i(\vec{G}_m \cdot \vec{r})} \qquad (2)$$

Then the Eq. (1) becomes a matrix eigenvalue equation.

$$(\nabla + i\vec{\beta}) \times \left[\frac{1}{\varepsilon}(\nabla + i\vec{\beta}) \times \sum_{m=1}^{N} h_m e^{i(\vec{G}_m \cdot \vec{r})}\right] = \left(\frac{\omega}{c}\right)^2 \sum_{m=1}^{N} h_m e^{i(\vec{G}_m \cdot \vec{r})} \quad (3)$$

We employ the conjugate gradient iterative minimization method for 3-D photonic crystal fiber structure with a large refractive index difference [13]. Following this method, the eigenvalue of the fundamental mode and its mode profile are obtained simultaneously by the minimization process of the energy functional defined as,

$$E_f(\vec{H}_{\vec{\beta}}) = \frac{1}{2} \frac{\int d^3r \vec{H}^*_{\vec{\beta}}(\vec{r}) \cdot \Theta \vec{H}_{\vec{\beta}}(\vec{r})}{\int d^3r \vec{H}^*_{\vec{\beta}}(\vec{r}) \cdot \vec{H}_{\vec{\beta}}(\vec{r})} \quad (4)$$

where $\Theta \equiv (\nabla + i\vec{\beta}) \times \left[\frac{1}{\varepsilon(r)}(\nabla + i\vec{\beta})\right] \times$ and $\vec{H}_{\vec{\beta}}(\vec{r}) = \sum_{m=1}^{N} h_m e^{i(\vec{G}_m \cdot \vec{r})}$.

To treat waveguiding structures along the z direction, we set the wavevector to have the form $\vec{\beta} = (0, 0, \beta_z)$. Once a fundamental mode is obtained, the higher-band eigenstates can be derived in ascending order by invoking the orthogonality condition. And to obtain the localized guided mode in the periodic structure, the supercell method is used [11]. The size of the supercell is chosen to be sufficiently greater than the mode size, then the coupling effect between the neighboring supercells is negligible.

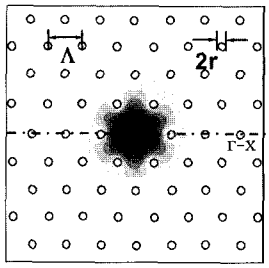

(a)

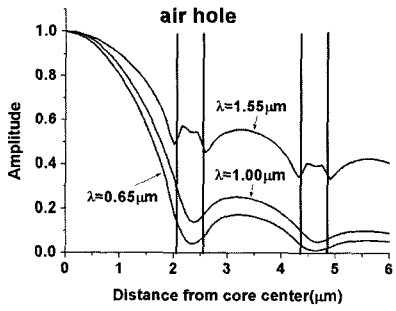

(b)

FIG. 1. Fundamental mode of a photonic crystal fiber ($r = 0.1\Lambda$, $\Lambda = 2.3$ μm, $n = 1.46$) (a) Mode profile at $\lambda = 0.65$ μm (amplitude contours, spaced by 10% of maximum value) (b) Cross-sectional field distributions along Γ - X direction shown in at three different wavelengths, $\lambda = 0.65$, 1.00, 1.55 μm.

As an example, we calculate the electric field profile of the fundamental mode of a hexagonal photonic crystal fiber with lattice constant $\Lambda = 2.3$ μm and refractive index $n = 1.46$. To ensure sufficient resolution we take the sampling space to be 2^5 grids per lattice constant. Thus when supercell size is $(N_x\Lambda) \times (N_y\Lambda) \times (N_z\Lambda)$, the number of planewaves are $(N_x \times 2^5)(N_y \times 2^5)(N_z \times 2^5)$. Here, N_x, N_y have to be chosen by considering the mode size and N_z determines the range of the wavevector along the z direction, i.e. $\beta_z = 0 \sim \pi/(N_z\Lambda)$. It takes about 20 seconds to calculate one fundamental eigenstate using a 1.0 GHz personal computer (AMD CPU) when we take the supercell size to be $7\Lambda \times 7\Lambda \times 0.1\Lambda$. Fig. 1(a) shows the fundamental mode calculated by the plane wave expansion method with air holes of radius $r = 0.1\Lambda$ at $\lambda = 0.65$ μm Fig. 1(b) shows that as the wavelength becomes longer, the effective size of the mode is enlarged and the field penetrates into the air holes resulting in a decrease of the effective index. However, at longer wavelengths, the penetration of the modal field becomes asymptotically saturated. This expansion of the mode profile is partly responsible for the spectrally wide single-mode nature of the photonic crystal fiber.

The dispersion relation can be easily obtained by varying the propagation wavevector along the z direction. In general, the effective index defined as β/k is one of the most important physical parameters for wave guiding structures. Fig. 2 shows the effective indices of PCFs with different air-hole sizes. To confirm the validity of the planewave expansion method, we also performed calculations based on three-dimensional(3-D) FDTD method [14]. The results obtained from the planewave expansion method are in good agreement with these 3-D FDTD results.

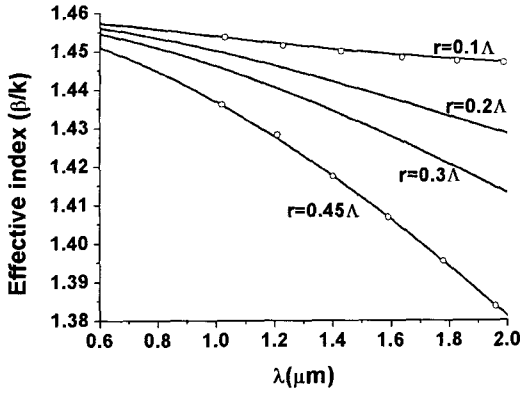

FIG. 2. Effective indices of photonic crystal fibers with different air holes ($\Lambda = 2.3$ μm, $n = 1.46$). The solid lines are the results of the plane wave expansion method and the open circles are obtained from the FDTD calculation.

These results also agree well with those previously obtained using the FEM [9].

The chromatic group velocity dispersion (GVD) is defined as the sum of the material dispersion D_m and the waveguide dispersion D_w:

$$D = D_m + D_w = -\frac{\lambda}{c}\left(\frac{d^2n}{d\lambda^2} + \frac{d^2n_{eff}}{d\lambda^2}\right) \qquad (5)$$

The waveguide dispersion is easily obtained from the effective index, n_{eff}, and the material dispersion can be calculated from the Sellmeier equation [15]. The resulting total group velocity dispersion for the fundamental mode of a silica photonic crystal fiber is plotted in Fig. 3, where the material dispersion of pure silica that has zero-crossing near 1.3 μm. According

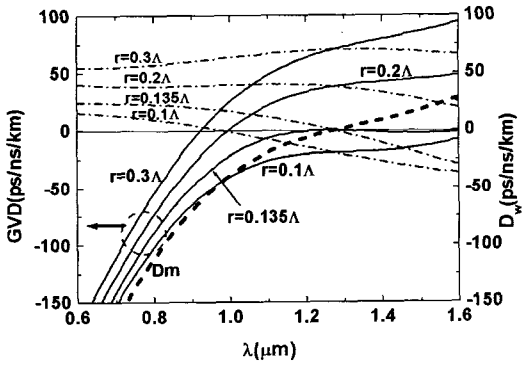

FIG. 3. Group velocity dispersion (GVD) for various air hole radii (solid lines). GVD is nearly zero over the range 1.2 $\sim$ 1.6 μm when the air hole radius is 0.135 Λ. Dash-dotted lines represent the waveguide dispersion D_w for each air hole size. Dotted line represents the material dispersion; it becomes zero $\sim$ 1.3 μm.(We selected supercell size as $12\Lambda \times 12\Lambda$ to certify the calculation accuracy sufficiently.)

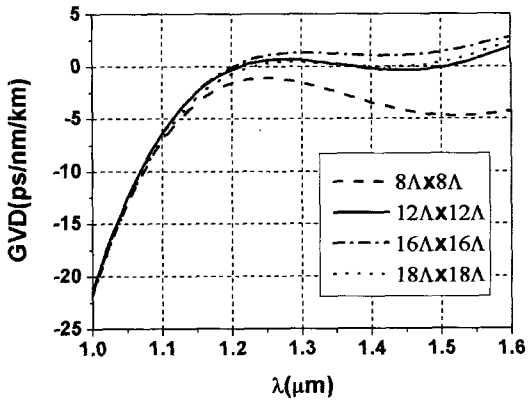

FIG. 4. The group velocity dispersion variation along to supercell sizes for the air hole radius $r = 0.135\Lambda$

to Fig. 3, when the size of the air hole is small, the waveguide dispersion curves have negative slopes with zero-crossings in the range 1.0 $\sim$ 1.5 μm. In particular, when the radius of the air hole is 0.135 Λ , the total GVD becomes very small over a wide spectral range (1.2 $\sim$ 1.6 μm). Similar results have been obtained previously using the FEM [16] and full vector technique [17]. However, if the size of the air hole becomes greater than 0.135 Λ, the waveguide dispersion becomes positive and the zero-crossing disappears within the interested wavelength range(1.3 $\sim$ 1.6 μm) [18].

Next, we investigate the effect of the supercell size. Fig. 4 represents the GVD variation for a PCF with $r = 0.135\Lambda$. One can see that the GVD does not depend strongly on the size of the supercell in the short wavelength region(<1.1 μm). In the long wavelength region, the result shows stronger dependence on the supercell size. However, the variation of GVD remains small(< 2 ps/nm/km) when the supercell size is larger than $12\Lambda \times 12\Lambda$.

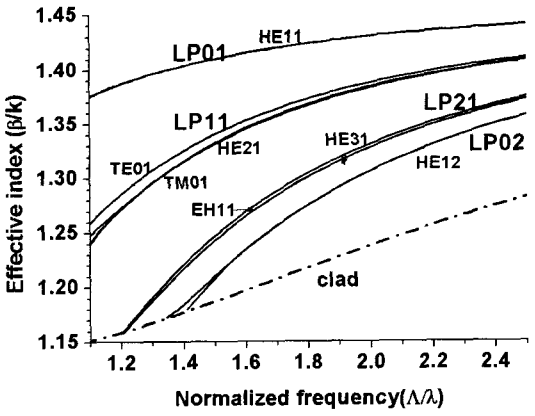

FIG. 5. The effective index of the higher-order modes ($\Lambda = 2.3$ μm, $r = 0.45\Lambda$)

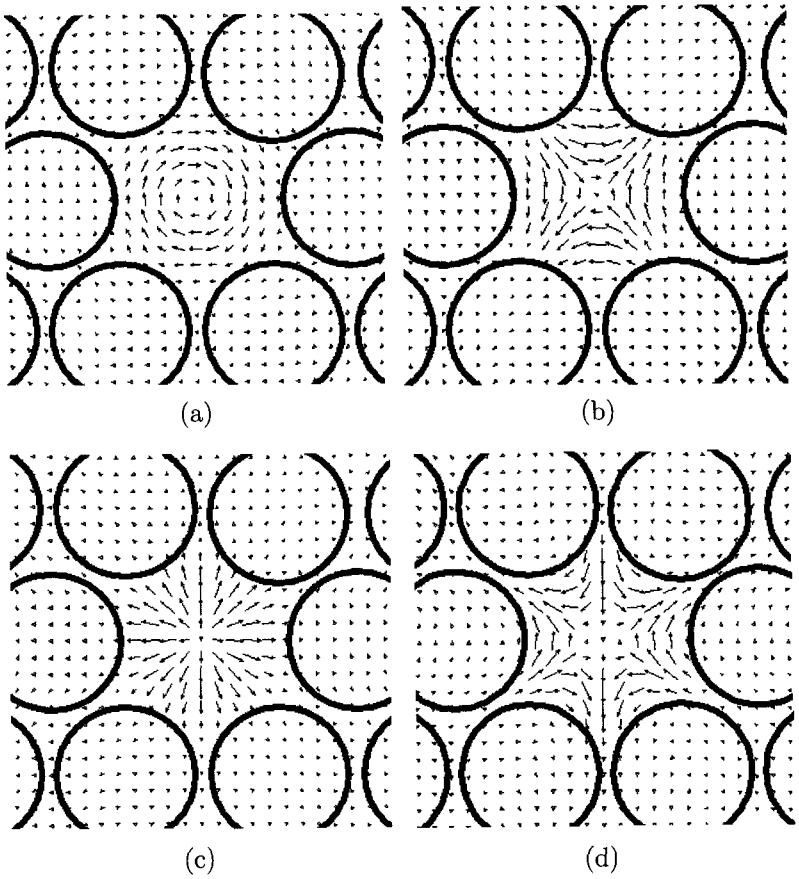

FIG. 6. The electric field distributions of higher-order modes at $\lambda = 1.55$ μm. (a) $TE_{01}(n_{eff} = 1.338)$ (b) $HE_{21}(n_{eff} = 1.330)$ (c) $TM_{01}(n_{eff} = 1.329)$ (d) $HE_{31}(n_{eff} = 1.243)$.

It is worth pointing out that the plane wave expansion method generates higher-order modes accurately and quickly compared to other methods. For example, Figs. 5 and 6 show the effective index and electric field of typical higher-order modes near λ =1.55 μm, respectively, for photonic crystal fibers of $r = 0.45\Lambda$. It is interesting to observe the presence of degenerate modes similar to those of the conventional fiber [19].

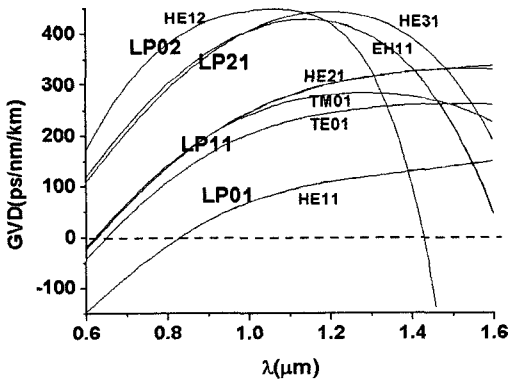

FIG. 7. The group velocity dispersion of the higher-order modes.

For example, doubly degenerate states such as the HE_{11}(x,y) modes and HE_{21}(even,odd) modes are observed. Following the methodology described above, the GVD of the higher modes can also be simply estimated (Fig. 7). Note that the position of the maximum GVD is blue-shifted because the influence of the air hole increases for the higher-order modes. It is also worth pointing out that the LP_{02} and LP_{21} groups have zero-crossing points within the spectral range of interest. In fact, the zero-crossing position can be adjusted by controlling the air hole size and material dispersion.

III. CONCLUSION

We calculated the modal characteristics of photonic crystal fibers using the plane wave expansion method. The plane wave expansion method is more than two orders of magnitude faster than the 3-D FDTD method, yet its results agree well with those of the FDTD method and the FEM method. The speed and accuracy of the proposed method should

see it widely used for the design of general high-index-contrast waveguide structures.

ACKNOWLEDGEMENT

This work was supported by the National Research Laboratory program of KISTEP.

*Corresponding author : yyjjlee@unitel.co.kr

REFERENCES

[1] O. J. Painter, R. K. Lee, A. Scherer, A. Yariv, J. D. O'Brien, P. D. Dapkus, and I. Kim, "Two-dimensional photonic band-gap defect mode laser," *Science*, vol. 284, pp. 1819-1821, 1999.

[2] H. Y. Ryu, S. H. Kim, S. H. Kwon, H. G. Park and Y. H. Lee, "Low threshold photonic crystal lasers from InGaAsP free-standing slab structures," *J. Opt. Soc. Korea*, vol. 6, pp. 57-63, 2002.

[3] J. C. Knight, T. A. Birks, P. St. J. Russell, and D. M. Atkin, "All-Silica single-mode optical fiber with photonic crystal cladding",*Opt. Lett.*, vol. 21, pp. 1547-1549, 1996.

[4] J. C. Knight, T. A. Birks, R. F. Cregan, P. J. Russell, and J. P. de Sandro, "Large mode area photonic crystal fibre," *Electron. Lett.*, vol. 34, pp. 1347-1348, 1998.

[5] D. S. Song, S. H. Kim, H. G. Park, C. K. Kim, and Y. H. Lee, "Single-fundamental-mode photonic-crystal vertical-cavity surface-emitting lasers," *Appl. Phys. Lett.*, vol. 80, pp. 3901-3903, 2002.

[6] A. Ferrando, E. Silvestre, J. J. Miret, and P. Andres, "Full-vector analysis of a realistic photonic crystal fiber," *Opt. Lett.* ,vol. 24, pp. 276-278, 1999.

[7] T. M. Monro, D. J. Richardson, N. G. R. Broderick, and P. J. Bennett, "Holey optical fibers: An efficient modal model," *IEEE J. of Lightwave Technol.*, vol. 17, pp. 1093-1102, 1999.

[8] T. M. Monro, D. J. Richardson, N. G. R. Broderick, and P.J. Bennett, "Modeling large air fraction holey optical fibers," *IEEE J. Lightwave Technol.* vol. 18, pp. 50-56, 2000.

[9] K. Saitoh, M. Koshiba, "Full-vectorial imaginary-distance beam propagation method based on a finite element scheme, application to photonic crystal fibers," *IEEE J. of Quantum Elecron.*, vol. 38, pp. 927-933, 2002.

[10] J. D. Joannopoulos, R. D. Meade, J. N. Winn, *Photonic Crystals*, (Princeton university press, Princeton, N. J., USA, 1995).

[11] S. G. Jonson, and J. D. Joannopoulos, "Block-iterative frequency-domain methods for Maxwell's equations in a plane wave basis," *Opt. Express.*, vol. 8, pp. 173-190, 2000.

[12] J. Broeng, S. Barkou, S. Thomas, B. Anders, "Analysis of air-guiding photonic bandgap fibers," *Opt. Lett.*, vol. 25, pp. 96-98, 2000.

[13] P.E. Gill, W. Murray, and M. H. Wright, *Practical Optimization*, (Academic, London, UK, 1981)

[14] The periodic boundary conditions and Berenger PML(perfectly matched layer) boundary condition are used for the propagating direction(z) and the transversal plane(x-y), respectively. And to increase the computational accuracy, the number of grids per lattice constant is set to 30 and the maximum time step is taken as 2^{16}.

[15] G. Ghosh, H. Yajima, "Pressure-dependent sellmeier coefficients and material dispersions for silica fiber glass," *IEEE J. of Lightwave Technol.*, vol. 16, pp. 2002-2005, 1998.

[16] F. Brechet, J. Marcou, D. Pagnoux, and P. Ray, "Complete analysis of the characteristics of propagation into photonic crystal fibers, by the finite element method," *Optical Fiber Technology*, vol. 6, pp. 181-191, 2000.

[17] A. Ferrando, E. Silvestre, J.J. Miret, P. Andres, "Nearly zero ultra-flatterned dispersion in photonic crystal fibers," *Opt. Lett.*, vol. 25, pp. 790-792, 2000.

[18] J. Kim, U. C. Paek, D. Y. Kim, Y. Chung, in *Optical Fiber Communication Conference '01*, Optical Society of America, Anaheim, USA, pp. WDD-86, 2001.

[19] A. Ferrando, E. Silvestre, J.J. Miret, P. Andres., "Vector description of higher-order modes in photonic crystal fibers," *J. Opt. Soc. Am. A*, vol. 17, pp. 1333-1339, 2000.